Binary fragmentations of excited nuclear systems in the 372 MeV Fe-56+Th-232 reaction

Binary fragmentations of excited nuclear systems in the 372 MeV ^{56}Fe + ^{232}Th reaction

P. K. Sahu,[1] R. G. Thomas,[1] A. Saxena,[1] R. K. Choudhury,[1,7] S. S. Kapoor,[1] L. M. Pant,[1] M. Barbui,[2] M. Cinausero,[2] G. Prete,[2] V. Rizzi,[2] D. Shetty,[2] D. Fabris,[3] M. Lunardon,[3] S. Moretto,[3] G. Viesti,[3] G. Nebbia,[3] S. Pesente,[3] B. Dalena,[4] G. D'Erasmo,[4] D. Di Santo,[4] E. M. Fiore,[4] M. Palomba,[4] A. Pantaleo,[4] V. Paticchio,[4] G. Simonetti,[4] N. Gelli,[5] F. Lucarelli,[5] A. Brondi,[6] and E. Vardaci[6]

[1]*Nuclear Physics Division, Bhabha Atomic Research Centre, Mumbai 400085, India*
[2]*Instituto Nazionale di Fisica Nucleare, Laboratori Nazionali di Legnaro, I-35020 Legnaro (Pd), Italy*
[3]*Dipartimento di Fisica and Sezione, Instituto Nazionale di Fisica Nucleare, Padova, I-35131 Padova, Italy*
[4]*Dipartimento Interateneo di Fisica and Sezione, Instituto Nazionale di Fisica Nucleare, Bari, I-70100 Bari, Italy*
[5]*Dipartimento di Fisica and Sezione, Instituto Nazionale di Fisica Nucleare, Firenze, I-50125 Firenze, Italy*
[6]*Instituto Nazionale di Fisica Nucleare and Dipartimento di Scienze Fisiche dell'Università di Napoli, I-80125 Napoli, Italy*
[7]*Institute of Physics, Bhubaneswar 751005, India*

(Received 22 April 2005; published 23 September 2005)

The binary fragmentation of the excited superheavy system of $Z = 116$ formed in the reaction 372 MeV ^{56}Fe + ^{232}Th has been investigated. The fragment masses and kinetic energies were determined through measurement of the fragment velocities by the time-of-flight method. Neutron spectra were measured in coincidence with the fragments at several angles with respect to the fragment direction, which were analyzed to deduce the total as well as the pre-scission neutron multiplicities. We analyzed the correlations between fragment mass and kinetic energy, gated and nongated by the coincidence with neutrons, to learn about the dynamics of the reaction with respect to the two-body exit channels. The events in the near-mass-symmetric valley region appear to receive a significant contribution from the asymmetric mode of fission of the superheavy compound nucleus $Z = 116$, which can be due to the influence of the closed proton and neutron shells of $Z = 50$ and $N = 82$ in the light fragments. From the observed number of pre-scission neutrons, it is inferred that the time scales of the fissionlike reactions leading to near-mass-symmetric splits are rather large, of the order of several times 10^{-20} s. The average number of prompt neutrons emitted in the spontaneous fission of such a superheavy nucleus is $\nu = (12 \pm 1)$, as deduced from the neutron measurements.

DOI: 10.1103/PhysRevC.72.034604 PACS number(s): 25.70. Jj

I. INTRODUCTION

In recent years, there has been great interest in studying the entrance-channel dependence of the fusion reactions between heavy ions, leading to compound nuclei formation in the superheavy region. Such studies can provide information on the dynamics of nucleus-nucleus collisions, which will help in the optimal selection of target-projectile combinations and bombarding energies to maximize the formation probability of superheavy nuclei as evaporation residues [1–8]. It is known that although asymmetric projectile-target combinations, such as a ^{48}Ca projectile on an actinide target, have a larger compound nucleus (CN) formation probability with respect to the case of a more symmetric projectile-target combination, the resulting CN is formed at a higher excitation energy in the former case. As a result, the fraction of compound nuclei leading to evaporation residue in such "hot-fusion" reactions becomes small because of the higher probability of multiple-chance fission as well as because of the washing out of nuclear shell effects at higher excitation energy. On the other hand, the so-called "cold-fusion" reactions involving more symmetric projectile-target combinations will lead to a smaller CN excitation energy and to a larger survival probability of the evaporation residues. However, in such cases there is a dynamical limitation to the CN formation, generally discussed in terms of "extra-push energy" [9], to push an intermediate dinuclear complex into a configuration more compact than the unconditional saddle point so that the dinuclear complex is trapped behind the fission barrier and evolves toward a compound nuclear shape. Detailed studies by Blocki *et al.* [10], based on one-body dissipation, show that the dynamical hindrance sets in when the product Z_pZ_T of the projectile-target charges becomes larger than a limiting value that ranges from 1000 to 1650, depending on the value of the charge asymmetry, Z_p/Z_T.

The main difficulty in the experimental study of the binary fragmentation of a superheavy CN stems from the fact that the two-body exit channels result predominantly from nonequilibrium fissionlike processes, namely, deep inelastic collision (DIC), quasi-fission (QF), and preequilibrium fission (PEF). The DICs involve shorter contact times and a smaller number of nucleon exchanges between the colliding partners, giving rise to mass distributions peaked around the projectile and target masses. The QF process involves much longer contact times and deeper penetration during collision with respect to DIC and results in a significant energy dissipation and transfer of mass and energy between reaction partners. In the case of a PEF process, the system is trapped into a configuration that is more compact compared with the unconditional saddle one, but it still reseparates as two fission fragments from an intermediate dynamical stage by diffusion over the barrier. The mass distributions of the nonequilibrium fission processes (for brevity, we refer to all nonequilibrium processes as QF in the rest of this paper) can extend toward

mass symmetry, approaching $A_{CN}/2$, where $A_{CN} = (A_p + A_T)$ is the mass of the composite system and A_p and A_T are the projectile and target masses, respectively. The mass-symmetric region may therefore be populated by both the CN-fission process and the QF process. It thus becomes difficult to separate the contributions of CN fission from the QF process on the basis of the fragment-mass distributions alone.

Measurements of fragment-mass–total-kinetic-energy (TKE) correlations and pre-scission and post-scission neutrons can provide a deeper insight into the reaction dynamics [11–15]. The total number of prompt neutrons emitted in the reaction is expected to depend on the available energy for a particular exit channel as well as the energy cost for emission of neutrons. This energy cost may depend on the shape of the emitting intermediate composite system and therefore on whether the reaction trajectories include the CN formation. The division of the total number of neutrons between the pre-scission and post-scission components is also expected to be dependent on the reaction dynamics. Hence neutron measurements are quite useful for learning about the nuclear dynamics involved in the formation of nuclei in the superheavy mass region.

In the present work, we report on an experiment devoted to the study of the $^{56}Fe + ^{232}Th$ reaction at 372 MeV bombarding energy. The correlations between the fragment mass and the TKE were obtained through two-body kinematics measurements with and without coincidence with emitted neutrons. Neutron spectra were measured at different angles in coincidence with the fission fragments and were analyzed to deduce pre-scission and post-scission neutron emission components. The details of the experimental setup and the data analysis procedure are described in Secs. II and III, respectively. The results are described in Sec. IV and discussed in Sec. V.

II. EXPERIMENTAL DETAILS

The experiment described in this work was performed at the heavy-ion accelerator facility of the Laboratori Nazionali di Legnaro by use of the experimental setup that was used in the past for a number of neutron measurements. A full description of the experimental system can be found in Ref. [16]. In the following text, only a few key features of the experimental setup are presented.

The 372 MeV ^{56}Fe beam from the Tandem XTU-ALPI superconducting linac with an intensity of 0.5–1 pnA was focused onto a self-supporting ^{232}Th target of thickness 1.5 mg/cm^2. The target was located at the center of a thin-walled (3-mm) spherical aluminum scattering chamber of 100-cm diameter.

The reaction products were detected in two time-of-flight (TOF) arms. One TOF arm consisted of a 3 cm × 5 cm parallel-plate avalanche counter (PPAC) placed at a distance of 7 cm from the target followed by a large-area (13.5 cm × 13.5 cm) position-sensitive multiwire proportional counter (MWPC1).

The flight path between the PPAC and the MWPC1 was 26 cm with a resulting opening angle $\Delta\theta_{lab} = \pm 11.5^\circ$. The PPAC was used to provide the start signal to measure the TOF in both the arms. The center of the first TOF arm was positioned at $\theta_{lab} = 65^\circ$, behind the reaction grazing angle. The second TOF arm consisted of another large-area (13.5 cm × 13.5 cm) position-sensitive MWPC2 placed at a distance of 15 cm from the target on the opposite side and centered at $\theta_{lab} = -65^\circ$, with an opening angle of $\pm 24^\circ$. The acceptance of the TOF arms allows the detection of coincident pairs of fragments from elastic scattering as well as from asymmetric and symmetric fragmentations of the composite system.

Neutrons were detected in 22 BC501 liquid scintillator cells each having 12.5-cm diameter and 12.5-cm thickness. Neutron detectors were placed around the scattering chamber at a distance of 2 m from the target. Twenty of them were placed in plane at the angles $\theta_{lab} = -35^\circ$, $\pm 45^\circ$, $\pm 55^\circ$, $\pm 65^\circ$, -75°, $\pm 45^\circ$, $+95^\circ$, $\pm 105^\circ$, $\pm 115^\circ$, $\pm 125^\circ$, $\pm 135^\circ$, -145°, -155°, and -165°, and two were placed out of plane with angles $\theta_{lab} = 53^\circ, \phi = +15^\circ$ and $\theta_{lab} = 53.7^\circ, \phi = -15^\circ$. The neutron TOF was measured-against the PPAC start signal. The absolute neutron TOF was determined with the γ-ray peak in the TOF spectrum as reference. The trigger of the data acquisition was generated by an OR signal of suitably prescaled fragment singles (defined as PPAC-MWPC1 coincidences), binary-fragment events (defined as PPAC-MWPC1-MWPC2 coincidences), and triple-coincidence events (defined by the coincidence of a two-fragment event with any of the neutron detectors). The data analysis was carried out with software tools based on the ROOT package, as previously done [17,18]. Neutron detector efficiencies were calculated with the experimentally determined thresholds of individual detectors, as described in Ref. [19].

III. DATA ANALYSIS

The data were analyzed to obtain various distributions and correlations of the two-fragment events in the exit channel of the reaction with and without coincidence with the emitted neutrons. The fragment TOF distributions in the two arms were calibrated by the selection of elastic-scattering events near the grazing angles. The fragment travel time over the 7-cm distance between the target and the PPAC was taken into account to convert the measured TOF into fragment velocities. Measured fragment velocities were also corrected for the energy loss in the target and in the PPAC detector foils (windows and electrodes that account for a total of 8 μm of Mylar) by use of range-energy tables. Fragment velocities measured in the laboratory were converted into center-of-mass velocities by application of kinematical transformations. Thus provisional fragment masses were obtained by application of the linear momentum and mass conservation relationships. Starting with the provisional masses, an iterative procedure was adopted that incorporated all the preceding steps from the measured TOF to determine new fragment masses and kinetic energies. The process was repeated to ensure convergence to final fragment masses and kinetic energies.

In the present study we analyzed only that class of events in which the lighter fragment, $A_{FF1} \leqslant (A_p + A_T)/2$, is entering the first TOF arm (PPAC-MWPC1). The other combination of events in which the complementary heavier fragment

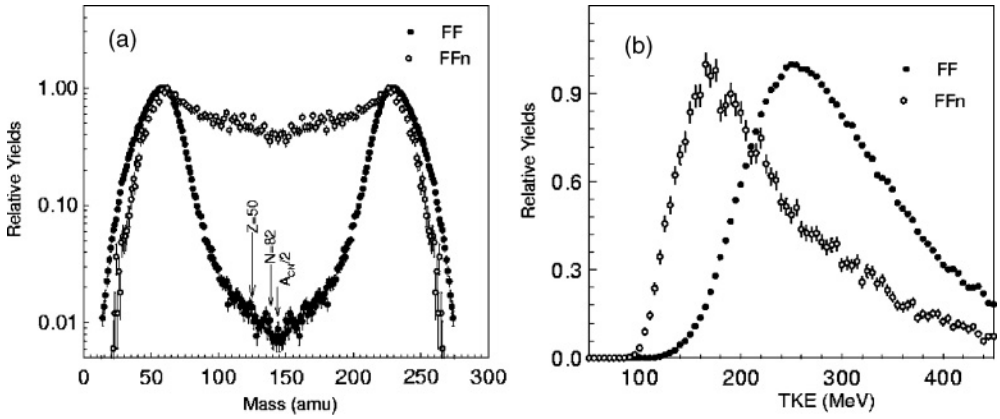

FIG. 1. (a)Fragment-mass and (b) TKE distributions for the 372 MeV ^{56}Fe + ^{232}Th reaction. Dots mark the binary-fragment events; open circles are used for fragment-neutron coincidences. The fragment masses corresponding to the closed proton $Z = 50$ shell, closed neutron $N = 82$ shell, and symmetric split are marked by arrows in Fig. 1(a).

$A_{\rm FF2} > (A_p + A_T)/2$ enters in this TOF arm is not analyzed because in this case the energy loss in the PPAC detector becomes substantially large, worsening the energy resolution of the apparatus. Thus, in the following text, results are obtained as a function of mass ratio $m_R = A_{\rm FF1}/(A_{\rm FF1} + A_{\rm FF2})$ with $m_R < 0.5$. For the sake of interpretation, the results have been reflected across $m_R = 0.5$ in some figures.

The recoil velocity $V_\parallel$ of the composite system parallel to the direction of the beam was determined from the measured folding angle and fragment velocities of each event, following the procedure given in Ref. [20]. The ratio $V_\parallel / V_{\rm CN,}$ where $V_{\rm CN}$ is the composite system velocity for full momentum transfer, was obtained as a function of fragment-mass ratio m_R. It is found that the $V_\parallel / V_{\rm CN}$ distribution is accounted for by a Gaussian function, centered at $V_\parallel / V_{\rm CN} \sim 1$ with a tail toward larger values. The events in the tail may have their origin in nonbinary events, such as the one arising from a three-body exit channel, when analyzed as binary considering only the two detected fragments. The presence of such events is significant because of the high fissility of the targetlike nuclei. In the analysis, the two-body events were selected by application of a proper gate on the measured $V_\parallel / V_{\rm CN.}$The width of the gate was taken to be 20% around the peak to account for the spread in $V_\parallel$ that was due to neutron evaporation.

IV. RESULTS

A. Fragment-mass, and TKE distributions and correlations

The observed fragment-mass distributions with and without coincidence with detected neutrons are shown in Fig. 1(a). The mass distribution extends all the way down to the symmetric exit channel ($m_R \sim 0.5$). It is seen that the symmetric valley is appreciably filled up in coincidence with neutrons, implying that the neutron emission increases significantly as one approaches the valley region corresponding to near-symmetric-mass division. This is expected as the energy ($E_{\rm c.m.} + Q_{\rm gg} -$ TKE) available for neutron emission increases with the increase in symmetry of the mass division. The observed TKE distributions with and without coincidence with the neutrons are shown in Fig. 1(b). Again, as expected, the number of emitted neutrons increases as a function of decreasing TKE, so that the requirement of coincidence with neutrons enhances the low TKE region of the distribution.

Fragment-mass distributions for selected TKE bins are shown in Fig. 2. These mass distributions are characterized by a strong peak close to the projectilelike masses and a valley in the region of near-symmetric-mass division. There is also an indication of a shoulder in the mass region of about 120–135 amu, which becomes more evident for the lower-TKE windows. In the hypothesis that the neutron-to-proton ratio *N/Z* in the fission fragment is equal to the compound nucleus one, the light fragment masses corresponding to the proton shell closure at $Z = 50$ and neutron shell closure at $N = 82$ are $A = 124$ amu and $A = 137$ amu, respectively. Such mass values are marked in Fig. 2 and Fig. 1(a) by arrows. The observed shoulder in the mass distributions can be interpreted as arising from mass asymmetric fission of the $Z = 116$ superheavy nucleus, and this mass asymmetry has its origin in the $Z = 50$, $N = 82$ closed proton and neutron shells of the light fragments.

We also carried out a detailed analysis of the correlation between fragment mass and TKE. Figure 3 shows the TKE distributions for few selected fragment-mass windows in the near-symmetric region. The arrows in Fig. 3 mark the calculated values of ($E_{\rm c.m.} + Q_{\rm gg}$) for each mass window.

The peak structure present in each distribution can be assigned to the binary splitting events. The high-energy tail that is prominently seen for the mass gate $A_{\rm FF1} = 131$–144 appears to be due to the residual three-body exit-channel events that may be still contaminating the selected $V_\parallel / V_{\rm CN}$ window. The main peak was fitted to a Gaussian distribution, and the first moment of the TKE distribution, $\langle$TKE$\rangle$, as a function of the detected fragment mass $A_{\rm FF1}$ is shown in Fig. 4. The region of fragment-masses $A_{\rm FF1} = 60$–100 amu is populated predominantly by DIC, and the TKE decreases with increasing $A_{\rm FF1}$, as expected. However, in the region of $A_{\rm FF1} = 100$–140 amu, the $\langle$TKE$\rangle$ increases again with $A_{\rm FF1}$, and the value of $\langle$TKE$\rangle$ measured for near-symmetric-mass

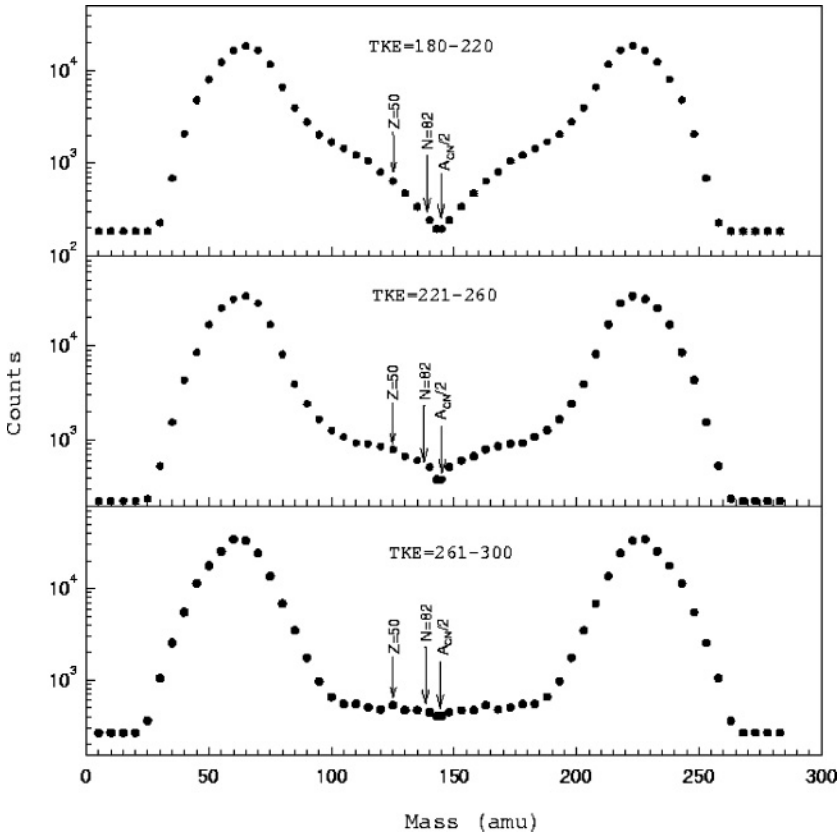

FIG. 2. Fragment-mass distributions for different TKE bins for the reaction 372 MeV ^{56}Fe + ^{232}Th.

splits ($A_{FF1} \sim 140$) is about 240 ± 5 MeV. For nearly mass-symmetric bins in the reactions of ^{64}Ni + ^{208}Pb and ^{238}U, which are populating composite systems with $Z_1 + Z_2 = 110$ and 120, Hinde *et al*. [12] have reported values of TKE of 237 and 266 MeV, respectively. Recently, for the reaction ^{58}Fe + ^{232}Th the values of ⟨TKE⟩ for mass-symmetric bins have been reported to be about 237 MeV by Itkis *et al*. [11]. It is to be noted that our experimental value of ⟨TKE⟩ is also very close to that expected from the systematics of Viola *et al*. for CN-fission events [21]. This fact is normally taken as an indication that a sizable part of the yield of symmetric splitting events might be from the CN-fission reaction mechanism, as also discussed in Ref. [11]. Figure 4 also shows the theoretical results of the heavy-ion collision dynamical calculations obtained with the HICOL. code, along with the values expected from the systematics of Viola *et al*., for comparison with the experimental results. There is reasonable qualitative agreement of the theoretical results with the experimental values for the kinetic-energy release as a function of the fragment mass.

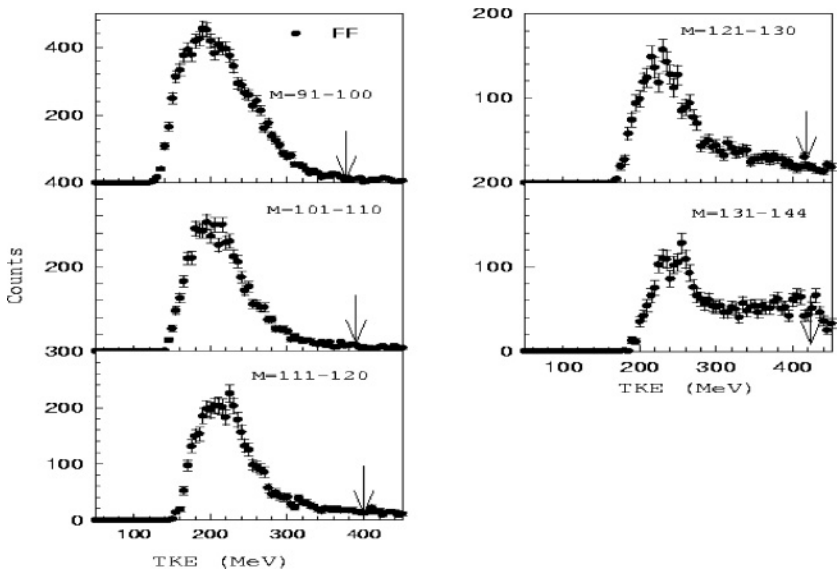

FIG. 3. Fragment TKE distributions for selected fragment-mass windows; the arrows mark the calculated $E_{c.m.} + Q_{gg}$ values for each mass window.

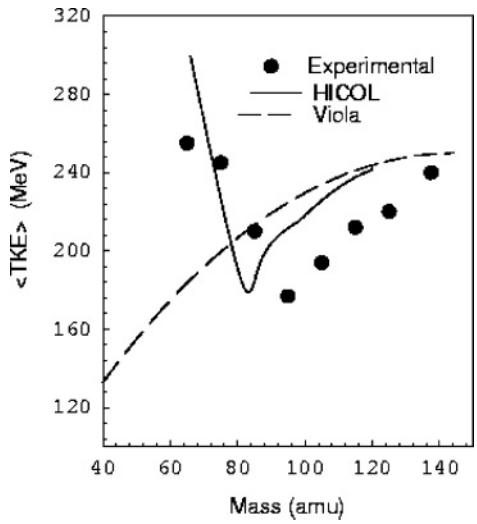

FIG. 4. Variation of fragment average total kinetic energy ⟨TKE⟩ with the mass of the detected fragment. The dashed curve corresponds to Viola's systematics [21]. The solid curve indicates predictions of the HICOL dynamical model [22].

B. Fragment-neutron coincidences

The coincident neutron spectra corresponding to different fragment- neutron angles were analyzed by a least-squares multisource fit routine, described in earlier papers [12,14,18], to determine the values of pre-scission neutron multiplicity ($\nu_{\rm pre}$), and the total number of emitted neutrons (ν_T). In this fitting procedure, the experimental velocity distributions of fragments were used, whereas the velocity of the composite system was set to the value corresponding to the full momentum transfer. The temperature $T_{\rm pre}$ of the composite system was determined by taking an average of the CN excitation energy and the excitation energy at scission with the level-density parameter $a = A/10$ MeV^{-1}. Fits to the experimental spectra were also checked by changing the $T_{\rm pre}$ value within 20% with respect to the preceding estmate to determine the effect of variation of the nuclear temperature that was due to the change of the available excitation energy during the descent from saddle to scission [12]. Typical fits to selected neutron spectra for the case of the fragment-mass window $A_{\rm FF1} = 130$–144 amu are shown in Fig. 5. The values of $\nu_{\rm pre}$ and ν_T obtained for different mass windows are shown in Fig. 6. The error bars on $\nu_{\rm pre}$ and ν_T include the statistical and fitting errors that are due to uncertainties in the emitting source temperature. It is seen that the value of ν_T increases from about $\nu_T = 1$ to $\nu_T = 25$ while going from the light fragment mass of $A_{\rm FF1} = 65$ amu to $A_{\rm FF1} = 115$ amu and remains roughly constant in the near-symmetric-mass region. On the other hand, the $\nu_{\rm pre}$is found to be almost zero for the masses up to $A_{\rm FF1} = 90$ amu and thereafter increases monotonically from about $\nu_{\rm pre} = 0$ to $\nu_{\rm pre} = 9$, going from mass $A_{\rm FF1} = 95$ amu to the symmetric split.

V. DISCUSSION

As mentioned earlier, the observed light fragment-mass distributions for selected TKE bins shown in Fig. 2 appear to be a superposition of two distributions comprising one large component peaked around the projectile mass and another small component leading to a shoulder in the mass region of 120–135 amu. We can interpret this feature as a first major component arising from the QF mechanism and a second small component contributed by the CN-fission mechanism. Our results indicate that CN fission of a super-heavy nucleus has an asymmetric mass distribution from the influence of $Z = 50$ and $N = 82$ closed shells in the light fragments. Itkis *et al*. [11] also interpreted their results on this basis for the reaction ^{58}Fe + ^{232}Th.

The observed variation of the average TKE, ⟨TKE⟩, with the fragment mass $A_{\rm FF1}$ presented in Fig. 4 has been interpreted with the help of model calculations. Dynamical trajectory calculations were performed based on the HICOL code [22,23], in which the dynamical evolution of the two colliding nuclei for different l values is described as a sequence of shapes, consisting of two spheres smoothly connected by a neck described by a quadratic surface of revolution. These calculations assume a one-body dissipation function, and the evolution is followed by the solution of the Langevin equations of motion. HICOL calculations predict that, for QF processes, the fragment-mass distribution in the present case can extend up to only $A_{\rm FF1} \sim 120$ amu. The results of HICOL calculations are in qualitative agreement with the experimental mass distribution, which is seen to extend all the way up to mass-symmetric division $(A_p+A_T)/2$. This again suggests the presence of a possible CN-fission component accounting for the near-symmetric masses. In the HICOL calculation, each l value gives a distinct contact time, a final mass asymmetry and TKE. One can also calculate TKE for various mass divisions from the HICOL code. Calculated values are shown in Fig. 4 as solid curves. Although the results of HICOL calculations bear a qualitative resemblance to the experimental ⟨TKE⟩ values, the experimental results feature somewhat lower kinetic energies with respect to the predicted values. This fact can be ascribed to the underestimation of the deformation effects in the calculations. Because HICOL calculations do not predict any CN formation cross section in the ^{56}Fe + ^{232}Th reaction, the calculated ⟨TKE⟩ versus mass corresponds to the QF mechanism alone. The dashed curve in Fig. 4 corresponds to the prediction of systematics by Viola *et al*. for CN fission [21]. The observed for the near-symmetric splitting is found to be close to the estimate of Viola *et al*., suggesting the presence of a possible CN-fission component.

We can further probe the reaction dynamics by using the $\nu_{\rm pre}$ values determined in the present experiment as a clock to estimate the dynamical time scales up to the scission point. For the near-symmetric-mass division window ($A_{\rm FF1} =$ 130–144 amu), we have deduced a value of $\nu_{\rm pre} = 9 \pm 1$ by using the procedure described earlier [17,18]. It is possible that both QF and CN-fission processes contribute to these near-symmetric-mass splits. In the first case the pre-scission neutrons are emitted during dynamical evolution from the point of initial contact to the final scission configuration. In the case of CN fission, the neutron emission can take place during the three stages involving the CN formation phase and CN-saddle and saddle-to-scission descent. In both cases, the bulk of the pre-scission neutron emission can come during the

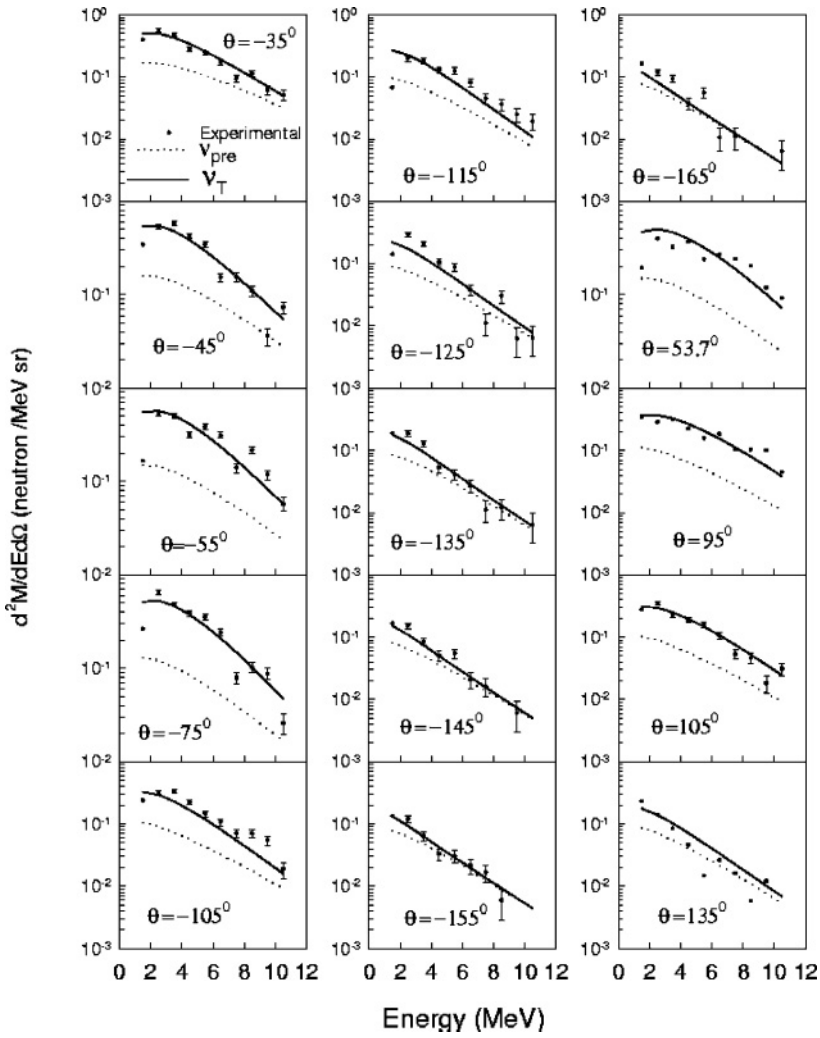

FIG. 5. Observed neutron spectra at different angles with respect to the beam direction for the fragment-mass window $A_{\mathrm{FF1}} = 130$–144 amu. Multisource fits to spectra are also shown: Solid curves correspond to the total neutron emission, and dotted curves correspond to the pre-scission neutron emission.

dynamical evolution of the dinuclear complex to the scission stage, when the excitation energy and the deformation are continuously changing. This makes it difficult to deduce a definite value for the emission time of the pre-scission neutrons.

However, it is still possible to obtain an estimate of the time scale of pre-scission neutron emission by making reasonable assumptions for the neutron binding energies, the level-density parameter, and the excitation energies of the emitting nuclei. The neutron binding energy B_n of the nucleus $^{288}116$ is calculated to be about 7.5 MeV for its normal spherical shape [24]. The value of B_n may become somewhat larger for the later stages of the pre-scission neutron emission cascade. On the other hand, for the elongated nuclear shapes, these values are estimated to become smaller by about 0.5 MeV [25]. To estimate the average initial excitation energy, one needs also to take into account additional heating of the nucleus that is due to partial conversion of the potential energy into thermal excitation energy during the passage of the nuclear system to the scission stage. The average value of this additional excitation energy has been estimated [14] to be about $0.6 \times Q_{\mathrm{eff}}$, where $Q_{\mathrm{eff}} = (Q_{\mathrm{fiss}} - \mathrm{TKE})$. In the present case for the symmetric-mass window of 130–144, Q_{eff} is about 103 MeV, with a value of 183 MeV taken for the mass excess of the $^{288}116$ nucleus [24]. This gives an average excitation energy of about 145 MeV corresponding to $(E_{\mathrm{CN}} + 0.6 \times Q_{\mathrm{eff}})$. With the average initial excitation energy of 145 MeV, the neutron emission times were calculated for the chain of neutron emission with the standard simplified expression [14] of the statistical model by use of level-density parameter $a = A/10\,\mathrm{MeV}^{-1}$ and the binding energy values $B_n = 7,\ 7.5$, and 8 MeV.

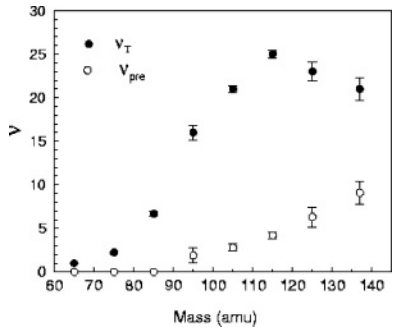

FIG. 6. Total and pre-scission neutron multiplicity as a function of light fragment mass A_{FF1} deduced from the fits to the measured fragment-neutron correlations.

The time scales corresponding to pre-scission neutron emission of $\nu_{\rm pre} = 8$, 9, and 10 are found to be: $(2.1 + 0.6 - 0.5) \times 10^{-20}$ s, $(2.6 + 1.6 - 0.6) \times 10^{-20}$ s and $(3.4 + 1.4 - 1.0) \times 10^{-20}$ s, respectively.

Thus it is reasonable to infer that the emission of the observed number of pre-scission neutrons for the selected mass window in the valley region would require a long time scale of several times 10^{-20} s. This long time scale indicates that observed mass yields in the valley region are contributed to significantly by CN fission.

For the near-symmetric-mass window of 130–144 amu, the value of $(E_{\rm c.m.} + Q_{\rm gg} - {\rm TKE})$ is about 185 MeV, taking the measured TKE value of 240 MeV. For this mass window the measured values of the pre-scission and total neutron multiplicities are $\nu_{\rm pre} = (9 \pm 1)$ and $\nu_T = (22 \pm 1)$, respectively. This gives an average energy cost of about (8.5 ± 0.5) MeV for the emission of a neutron, including both pre-scission and post-scission stages. One expects that this energy cost will be somewhat different for the pre-scission and post-scission stages because of differences in both neutron binding energies and source temperatures in the two cases. In the absence of more detailed information on these values, we assume that the preceding value of the average energy cost is a good approximation also in case of pre-scission neutron emission. With this assumption, the excitation energy at scission for the preceding symmetric-mass window is estimated to be about (109 ± 10) MeV, corresponding to the emission of about $\nu_{\rm post} = (13 \pm 1)$ post-scission neutrons. For the more asymmetric mass windows of $A_{\rm FF1} = 120$–129 amu and $A_{\rm FF1} = 110$–119 amu, for which the post-scission neutrons are about $\nu_{\rm post} = 16$ and $\nu_{\rm post} = 20$, the estimated available excitation energy at scission comes out to be about 139 and 154 MeV, respectively. Thus the available energy for post-scission neutron emission is smallest in the near-symmetric valley region of the mass distribution.

Using the mass difference value of 183 MeV for the superheavy nucleus $^{288}116$ [24], the effective Q value, $Q_{\rm eff} = (Q_{\rm fiss} - {\rm TKE})$ for the mass window $A_{\rm FF1} = 130$–144 amu is estimated to be about 103 MeV. This value is quite close to the estimated residual energy of (109 ± 10) MeV available for particle emission at scission after the emission of pre-scission neutrons, even though the initial excitation energy of the CN is estimated to be about $E_x = 82$ MeV. For more asymmetric mass divisions, the available energy at scission is estimated to be significantly larger than the corresponding $Q_{\rm eff}$ values. Thus these near-symmetric-mass divisions seem to arise from relatively colder scission configurations resulting from the cases in which the initial excitation energy has been drained off by the pre-scission neutrons. On the basis of the preceding observed post-scission neutron multiplicity for the near-symmetric-mass window, corresponding to the estimated available energy of (109 ± 10) MeV at scission, the average number of neutrons corresponding to the excitation energy at scission of $Q_{\rm eff} = 103$ MeV comes out to be (12 ± 1). In other words, the average number of neutrons expected to be emitted in the spontaneous fission of a superheavy nucleus $^{288}116$ is $\nu = (12 \pm 1)$.

VI. SUMMARY AND CONCLUSIONS

The present study of the 372 MeV ^{56}Fe + ^{232}Th reaction has shown that, although the bulk of the events corresponds to QF, there exists a small component of binary events, which may arise from mass-asymmetric fission of the CN. Such a fission process seems to be influenced by the $Z = 50$ and $N = 82$ closed proton and neutron shells in the light fragment. This observation is also supported by the measured $\langle {\rm TKE} \rangle$ values, which are close to the systematics of Viola *et al.* for this class of events.

The measured pre-scission neutron multiplicity for the near-symmetric events is $\nu_{\rm pre} = 9 \pm 1$, which corresponds to a large time scale of several emission times 10^{-20} s.

As pointed out earlier, for the superheavy nucleus $^{288}116$ [24], the effective Q value, $Q_{\rm eff} = (Q_{\rm fiss} - {\rm TKE})$ for the mass window $A_{\rm FF1} = 130$–144 amu is estimated to be about 103 MeV. The excitation energy deduced from the measured pre-scission and total neutron multiplicities for the near-symmetric-mass region is seen to be close to the effective value of the excitation energy at scission, $Q_{\rm eff}$, of the super heavy nucleus, although the initial excitation energy for the CN is quite large ($E_x \sim 83$ MeV). This implies that most of the initial excitation energy has been taken away by the emission of neutrons in the pre-scission stage. From our experimental data, the average neutron multiplicity for the case of spontaneous fission of the superheavy nucleus $^{288}116$ is estimated to be about $\nu = 12 \pm 1$.

ACKNOWLEDGMENTS

Technical support from M. Caldogno (Padova) and from G. Antuofermo, G. Iacobelli, M. Sacchetti and P. Vasta (Bari) during the experiment is gratefully acknowledged. Thanks are due to the staff of Laboratori Nazionali di Legnaro for the excellent beams provided. This work was performed under the BARC-INFN Collaboration.

[1] Y. Aritomo, T. Wada, M. Ohta, and Y. Abe, Phys. Rev. C **59**, 796(1999); Y. Abe, Eur. Phys. J. A **13**, 143 (2002).
[2] M. Bender *et al.*, Phys. Lett. **B515**, 42 (2001).
[3] G. G. Adamian, N. V. Antonenko, and W. Scheid, Phys. Rev. C **68**, 034601 (2003).
[4] A. S. Zubor *et al.*, Phys. Rev. C **65**, 024308 (2002).
[5] M. G. Itkis *et al.*, Phys. Rev. C **65**, 044602 (2002).
[6] V. Ninov *et al.*, Phys. Rev. Lett. **83**, 1104 (1999); **89**, 039901 (2002).
[7] Yu. Oganessian *et al.*, Nature (London) **400**, 242 (1999); Eur. Phys. J. A **15**, 201 (2002).
[8] Y. Aritomo and M. Ohta, Nucl. Phys. **A744**, 3 (2004).
[9] W. J. Swiatecki, Phys. Scr. **24**, 113 (1981); S. Bjornholm and W. J. Swiatecki, Nucl. Phys. **A391**, 471 (1982) .

[10] J. F. Blocki *et al*., Nucl. Phys. **A459**, 145 (1986).
[11] See M. G. Itkis *et al*., Nucl. Phys. **A734**, 136 (2004) and references therein.
[12] D. J. Hinde *et al*., Phys. Rev. C **45**, 1229 (1992).
[13] L. Donadille *et al*., Nucl. Phys. **A656**, 259 (1999).
[14] D. Hilscher and H. Rossner, Ann. Phys. (Paris) **17**, 471 (1992).
[15] T. Materna *et al*., Nucl. Phys. **A734**, 184 (2004).
[16] See L. Fiore *et al*., Nucl. Phys. **A620**, 71 (1997) and references therein.
[17] A. Saxena *et al*., Phys. Rev. C **65**, 064601 (2002).
[18] A. Saxena *et al*., Nucl. Phys. **A730**, 299 (2004).
[19] A. Pantaleo *et al*., Nucl. Instrum. Methods A **291**, 570 (1990).
[20] E. Mordhorst *et al*., Phys. Rev. C **43**, 716 (1991).
[21] V. E. Viola, K. Kwiatkowski, and M. Walker, Phys. Rev. C **31**, 1550 (1985).
[22] H. Feldmeier, Rep. Prog. Phys. **50**, 915 (1987).
[23] K. Kumar, R. K. Choudhury, and A. Saxena, Pramana J. Phys. **42**, 123 (1994).
[24] R. Smolanzuck, Phys. Rev. C **56**, 812 (1997).
[25] J. P. Lestone *et al*., Phys. Rev. Lett. **70**, 2245 (1993).